communications chemistry

Article

https://doi.org/10.1038/s42004-024-01128-z

Dual-controlled guest release from coordination cages

Check for updates

Yuqing Yao[1,2], Chengyuan Shao[1,2], Shuwei Wang[1], Qiufang Gong[1], Jia Liu[1], Hua Jiang[1] ✉ & Ying Wang[1] ✉

Despite having significant applications in the construction of controlled delivery systems with high anti-interference capability, to our knowledge dual-controlled molecular release has not yet been achieved based on small molecular/supramolecular entities. Herein, we report a dual-controlled release system based on coordination cages, for which releasing the guest from the cage demands synchronously altering the coordinative metal cations and the solvent. The cages, $\mathbf{Hg_5L_2}$ and $\mathbf{Ag_5L_2}$, are constructed via coordination-driven self-assembly of a corannulene-based ligand. While $\mathbf{Hg_5L_2}$ shows a solvent-independent guest encapsulation in all the studied solvents, $\mathbf{Ag_5L_2}$ is able to encapsulate the guests in only some of the solvents, such as acetone-d_6, but will liberate the encapsulated guests in 1,1,2,2-tetrachloroethane-d_2. $\mathbf{Hg_5L_2}$ and $\mathbf{Ag_5L_2}$ are interconvertible. Thus, the release of guests from $\mathbf{Hg_5L_2}$ in acetone-d_6 can be achieved, but requires two separate operations, including metal substitutions and a change of the solvent. Dual-controlled systems as such could be useful in complicated molecular release process to avoid those undesired stimulus-responses.

Capabilities regarding the controlled release of chemical substances are crucial for many applications, including drug delivery[1], gene transfection carriers[2], controllable catalysis[3], and stimuli-responsive functional materials[4]. In the past decades, various entities, from the macroscopic capsules[5] to polymers[6] and molecular assemblies[7,8], have been designed as carriers for controlled releasing drugs or chemicals. Recently, attention has been devoted to the systems with complicated release functions[9].

Supramolecular cages possess a rigid and isolated (fully or partially) three-dimensional inner space[10,11]. Though such a structural characteristic is greatly beneficial for molecular encapsulation and provides the cages special potentials in reactive intermediate storages[12,13], catalysis[14], purification[15,16], etc., it gives, on the other hand, the controlled release of the encapsulated guests when required being quite challenging. Nonetheless, substantial progress has still been made. A widely used approach in this regard is the disassembly of the cage architectures[17–26]. Besides, competitive molecules (including solvents) were also used for expelling the guests included[27–31]. Other rational designs include denaturing the cages/guests for a significant decrease of the host–guest affinities by various stimuli, such as light[32–36], metal-coordinations[37,38], electrolyte[39], transmetallation[40], redox[41–43], reactions[44,45] and changes in pH[46–48] or temperatures[43,49,50]. Despite these elegant studies demonstrated a high efficiency in release of guests, the releases themselves typically respond to only a single stimulus, leaving cage systems that can realize precisely controlled release in complicated situations unexplored to a large extent.

Dual control is a regulation that requires at least two separate control strategies operating in concert to perform a task (Fig. 1a). Dual control process has been widely used in high-risk areas of bank transaction[51] and mechanical engineering[52,53] to protect information or sensitive functions. In biology, it is adopted to generate a single, integrated response while information from several different sources is received simultaneously[54,55]. Theoretically, employment of such a dual-modality in controlled release would eliminate the uniqueness of the relevance of the release to a certain stimulus, reducing the correlation between the release and other functions relating to the particular stimulus, thus helping to construct anti-interference guest-release systems that are crucial for many applications of such systems in the future, including the drug delivery, gene transfection carriers and controllable catalysis. To date, a few dual-controlled systems have been constructed based on polymers/biopolymers[56,57] and mesoporous nanoparticles[58–60] for liberating drugs and chemicals[61,62]. Nevertheless, establishing such a function based on small molecular/supramolecular entities remains an unmet challenge.

Herein, we present, to the best of our knowledge, the first example of a dual-controlled guest release system based on coordination cages, using 1,3,5,7,9-penta(2,2'-bipyridin-5-yl)corannulene (**1**) as the ligand (Fig. 1b). We show that the complexation of **1** with Hg(II) and Ag(I) cations can produce two kinds of well-defined cage complexes, $\mathbf{Hg_5L_2}$ and $\mathbf{Ag_5L_2}$. Whereas the $\mathbf{Hg_5L_2}$ cages show a solvent-independent guest encapsulation

[1]College of Chemistry, Beijing Normal University, Beijing 100875, P. R. China. [2]These authors contributed equally: Yuqing Yao, Chengyuan Shao.
✉e-mail: jiangh@bnu.edu.cn; ywang1@bnu.edu.cn

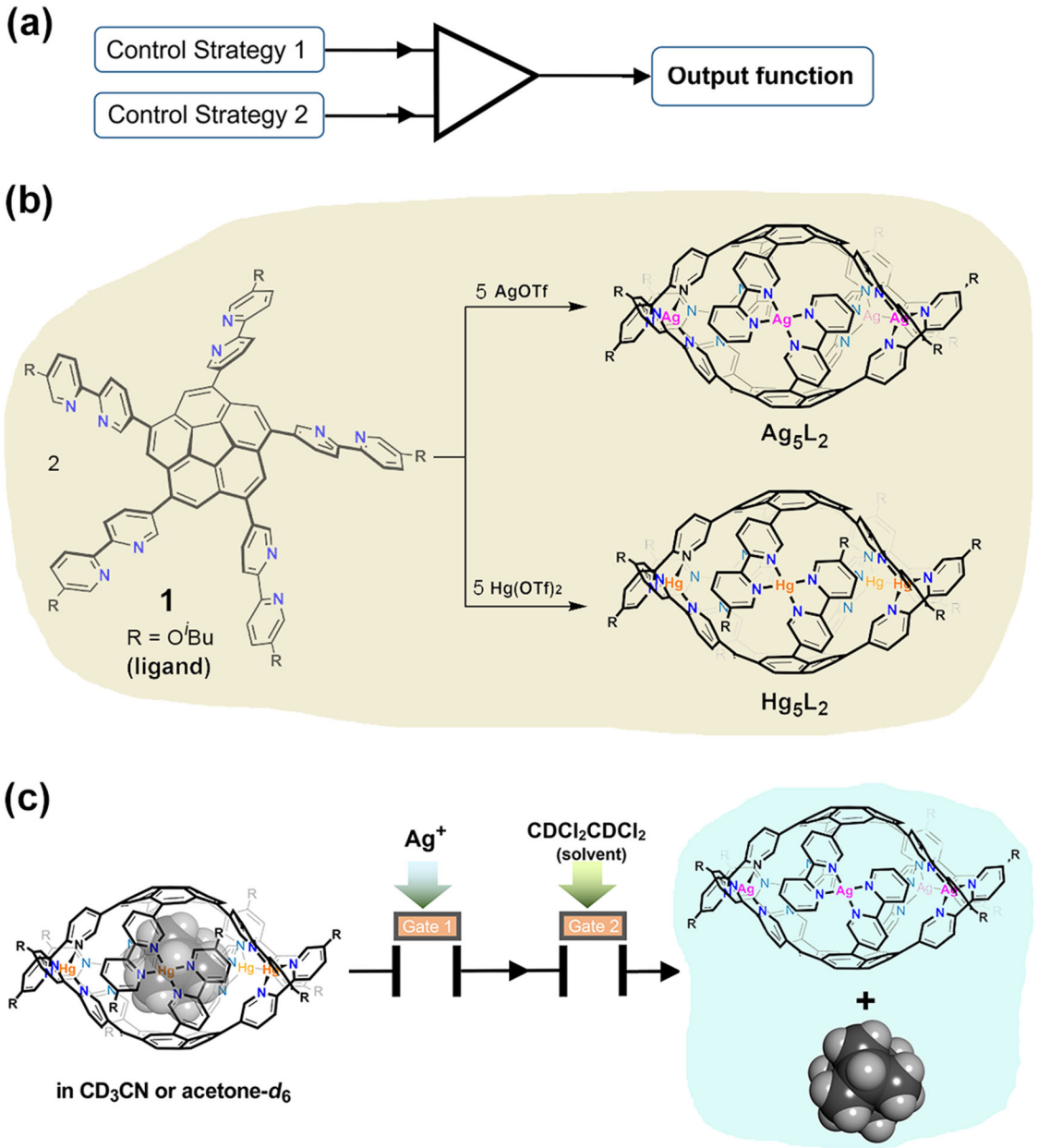

Fig. 1 | Overview of the dual-controlled guest release from cages. a Schematic representation of the dual control processes, in which two control strategies operate in concert to perform tasks. **b** The corannulene-based ligand **1** and the self-assembly to cages $\mathbf{Hg_5L_2}$ and $\mathbf{Ag_5L_2}$. The convex-*P,M,P* conformers of the cages are shown as examples. **c** Schematic representation of the dual-controlled guest release system studied herein, for which releasing the guest from $\mathbf{Hg_5L_2}$ demands synchronous alteration of the coordinative metal cations and the solvent.

in the studied cases, the guest encapsulation and release from $\mathbf{Ag_5L_2}$ are controlled by the solvents. These two kinds of cages are interconvertible through transmetallation, thus giving the guest release from $\mathbf{Hg_5L_2}$ to be dually regulated by the metal cations and the solvents (Fig. 1c), while the liberation from $\mathbf{Ag_5L_2}$ ones is solvent-gated only. Dual-controlled systems, as such, may find applications in complicated cargo release process[63].

Results and discussion

Design and synthesis

Different from those cage systems undergoing significant structural and geometric changes upon stimuli[64], the ones we attempted to obtain are supposed to change moderately in the cavity shape and volume upon the changes of complexed metal ions. Such features would allow the cages to alter their host capabilities moderately while concurrently maintaining the overall binging inclinations, thus facilitating fine-tuning of their guest-binding behaviors. In this regard, we were drawn to the molecular cages constructed by coordination-driven self-assembly with two high-symmetry building blocks[65]. Within such kind of cages, the metal components are limited in number and therefore function more like a simple linker rather than an important assembly organizer (as that in cages assembled from many small chelating ligands[66]). As a result, changing the coordinated metal cations would give rise to moderate changes in the size, shape, and other properties of the capsular inner space.

Corannulene is an excellent building block for constructing molecular cages due to the C_{5v} symmetry in its structure and the high reactivity[67]. In particular, corannulene possesses a curved π-surface and a dynamic, switchable molecular chirality in solution[68], which can provide theoretically the corresponding cages a lot of intriguing properties that are in sharp contrast to those assembled via planar π-conjugated systems[67,69]. Nevertheless, the properties of corannulene-based molecular cages, including

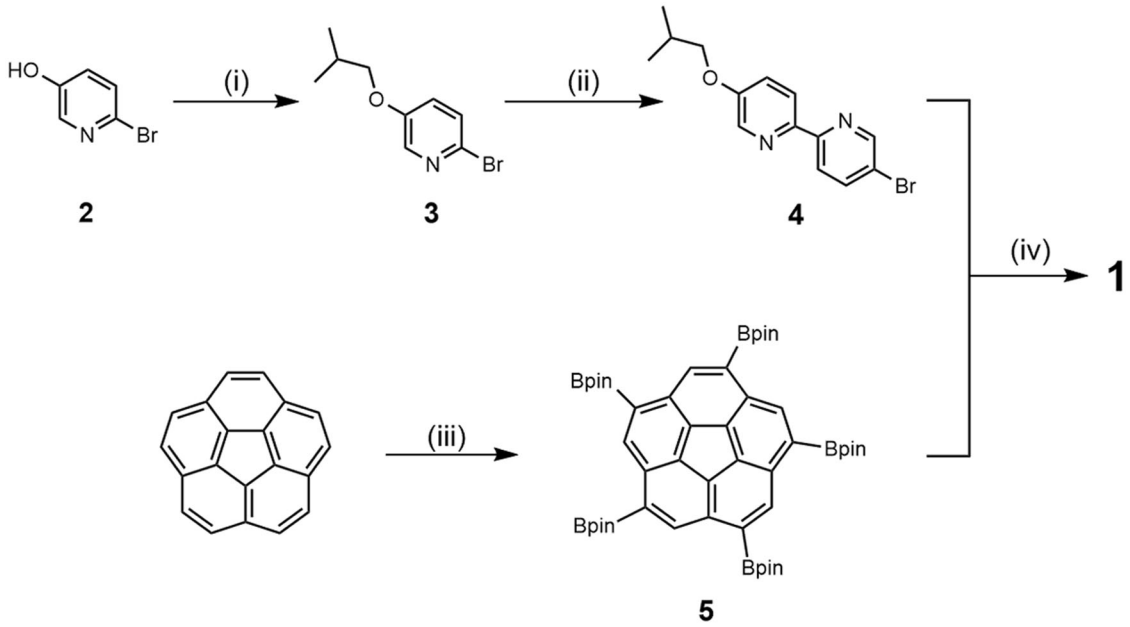

Fig. 2 | Synthesis of Ligand 1. Reagents and conditions: (i) 1-iodo-2-methylpropane, K_2CO_3, DMF, 60 °C, 8 h (50%); (ii) *n*-BuLi, $ZnCl_2$, 2,5-dibromopyridine, $Pd(PPh_3)_4$, THF, reflux, 24 h (32%); (iii) $[Ir(OMe)COD]_2$, 4,4'-dimethyl-2,2'-bipyridyl, B_2pin_2, potassium *t*-butoxide, THF (80%); (iv) $Pd(PPh_3)_4$, K_2CO_3, benzene/methanol/water, 100 °C, 4 d (68%).

those in the aspect of host–guest interactions, had not been examined for quite a long time. We recently reported the first example of corannulene-based molecular cage[70,71], constructed by coordination-driven self-assembly of 1,3,5,7,9-penta(pyridyl-3-yl)corannulene ligands and Ag^+ cations. However, this cage is not suitable for the present purpose because the involved linear bidentate coordination is, to some extent, unfavorable to the modulation of the inner cavity due to the lack of diversity in the coordination pattern. We, therefore, envisioned substituting 2,2'-bipyridin-5-yl (bpy) groups for the pyridyl-3-yl ones on the ligand. Given the presence of various coordination geometries for metal cations with coordination numbers four or six, we expected that, by deliberate choice of metal species, overall the size/shape of the inner cavity could be tuned, thus providing an effective strategy towards controlling guest encapsulations. An *iso*-butoxy side chain was introduced on the tail of each bpy unit for enhanced solubility.

Our synthetic approach to the bpy ligand is outlined in Fig. 2. Initially, *O*-alkylation of 2-bromo-5-*iso*-butoxypyridine (**2**) with alkyl iodide provided **3**. Treatment of **3** with *n*-BuLi and $ZnCl_2$ generated the organozinc in situ, which then underwent Negishi cross-coupling reaction to give **4**. Finally, the Suzuki coupling of **4** with 1,3,5,7,9-pentakis(Bpin)corannulene (**5**) provided the target ligand **1** (Supplementary Methods 1 and 2; Supplementary Data). The structure of **1** was confirmed by nuclear magnetic resonance (NMR) and high-resolution mass spectra. (see Supplementary Figs. 14−17 and 30 in the Supplementary Information (SI)).

Metal complexation and the formation of Ag_5L_2 and Hg_5L_2 cages

To explore the feasibility of access to the desired cages and to expand the pool of suitable metal cations, several kinds of metal ions with the potential to coordinate bpy to form four- or six-coordinate complexes[72], including Ag^+, Hg^{2+}, Fe^{3+}, Cu^+, Mg^{2+}, Ni^{2+}, and Zn^{2+} ions, were first preliminarily screened. Mixing **1** with $Fe(OTf)_3$, $Ni(ClO_4)_2$, $Zn(OTf)_2$ or $Zn(ClO_4)_2$ at the ratio of 2:5 (mol/mol) in common solvents or solvents mixture gave no or extremely broad signals in the ^{1}H NMR spectra, even after the samples were heated at elevated temperature (Supplementary Fig. S1). When the ligand was combined with $Mg(OTf)_2$, no obvious changes were observed, indicative of the absence of coordination. With AgOTf, $Hg(OTf)_2$ or $Cu(CH_3CN)_4PF_6$ as the salt, in the solvent mixture of $CD_3CN/CDCl_3$, the ^{1}H NMR spectrum showed a new set of intense signals (Supplementary Figs. 1 and 2), suggestive of a promising formation of well-defined cage complexes. However, the Cu^+ cages tend to decompose under ambient conditions, as evidenced by the disappearance of its ^{1}H NMR signals in three hours. The Ag^+ and Hg^{2+} complexes are stable enough in solutions; we thus mainly focused on these two cations in the following studies.

It is noteworthy that while both Ag^+ and Hg^{2+} cations possess the ability to form complexes of several different coordination numbers, they have a flexible coordinating sphere, thus having weak coordination geometry preferences and being able to tolerate, to some extent, the distortion from the ideal geometries[73,74], which may contribute to the formation of stable molecular cages in the studied cases. Besides, Ag^+ and Hg^{2+} complexes favor associative ligand exchanges. This character would promote the interconversion between different structures/configurations (if they exist) and greatly help the complexes to rapidly reach the most favourite ones.

Theoretically, the inherent chirality of corannulene causes the existence of four different stereo configurations (*P,M,P/M,P,M* and *P,P,P/M,M,M*)[70] for the desired Ag^+ and Hg^{2+} cages. In addition, due to the long bpy substituents as well as the possible bowl-to-bowl inversion of the corannulene moieties, the cages, on the whole, may adopt a clam-shell-like, biconvex structure, or a sunken, biconcave-lens-like geometry[75]. Therefore, totally eight stereoisomers (containing four pairs of enantiomers) are imaginable for each cage, including biconvex-*P,M,P/M,P,M* and biconvex-*P,P,P/M,M,M* as well as biconcave-*P,M,P/M,P,M* and biconcave-*P,P,P/M,M,M*. For better understanding of the relationships between different isomers, density functional theory (DFT) (B3LYP-D3(BJ)//LANL2DZ/6-31 G(d)) calculations[76] were carried out. Careful examinations revealed the possible existence of three pairs of enantiomers for the isolated $[Ag_5\mathbf{1}_2]^{5+}$ cage, including biconvex-*P,M,P/M,P,M*, biconvex-*P,P,P/M,M,M* and biconcave-*P,M,P/M,P,M*; for $[Hg_5\mathbf{1}_2]^{10+}$, two pairs are obtained as minima, including biconvex-*P,M,P/M,P,M* and biconcave-*P,M,P/M,P,M* (Fig. 3, Supplementary Method 15 and Supplementary Tables 15–17, SI). The other stereoisomers do not represent any minima (local or global) on the corresponding potential energy surface. For examples, optimizations starting from biconcave-(*P,P,P/M,M,M*)-$[Ag_5\mathbf{1}_2]^{5+}$ and biconvex-(*P,P,P/M,M,M*)-$[Hg_5\mathbf{1}^2]^{10+}$ will give rapidly the geometries of biconvex-(*M,P,M/P,M,P*)-$[Ag_5\mathbf{1}_2]^{5+}$ and biconcave-(*M,P,M/P,M,P*)-$[Hg_5\mathbf{1}_2]^{10+}$, respectively.

The energy-minimized structures of all the obtained stereoisomers of $[Ag_5\mathbf{1}_2]^{5+}$ and $[Hg_5\mathbf{1}_2]^{10+}$ possess a helical, D_5-symmetric geometry. Notably, the biconcave configuration is, to some extent, conducive to releasing

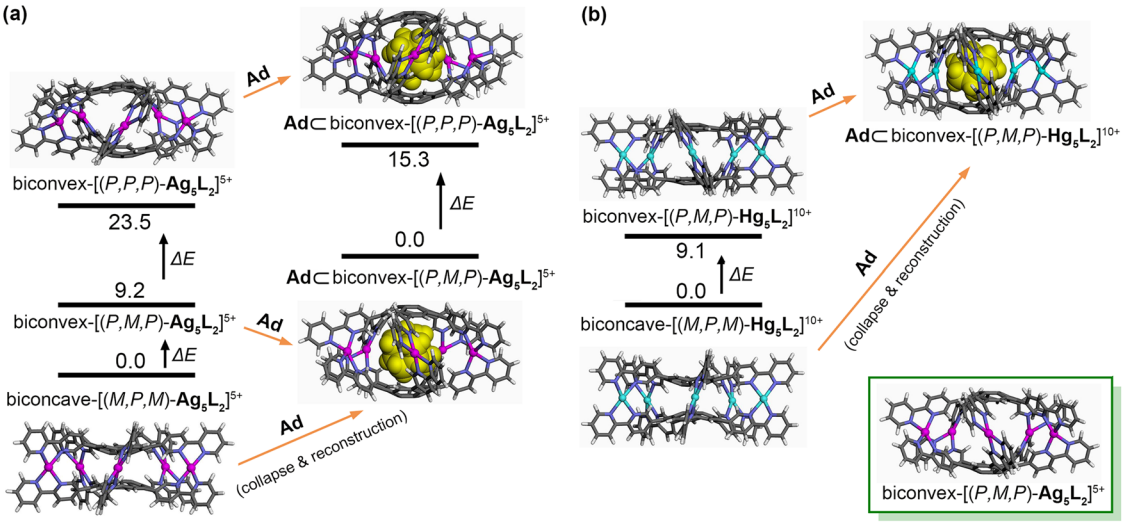

Fig. 3 | DFT (B3LYP-D3(BJ)//LANL2DZ/6-31 G(d)) energy-minimized structures. a Five species relating to the Ag^+ cages, including biconvex-[(*P,P,P*)-$\mathbf{Ag_5L_2}$]$^{5+}$, biconvex-[(*P,M,P*)-$\mathbf{Ag_5L_2}$]$^{5+}$, biconcave-[(*M,P,M*)-$\mathbf{Ag_5L_2}$]$^{5+}$, **Ad**⊂biconvex-[(*P,M,P*)-$\mathbf{Ag_5L_2}$]$^{5+}$, and **Ad**⊂biconvex-[(*P,P,P*)-$\mathbf{Ag_5L_2}$]$^{5+}$. The inset (bottom right corner) shows a side-viewed structure of biconvex-[(*P,M,P*)-$\mathbf{Ag_5L_2}$]$^{5+}$. **b** Three species relating to the Hg^{2+} cages, including biconvex-[(*P,M,P*)-$\mathbf{Hg_5L_2}$]$^{10+}$, biconcave-[(*M,P,M*)-$\mathbf{Ag_5L_2}$]$^{10+}$ and **Ad**⊂biconvex-[(*P,M,P*)-$\mathbf{Hg_5L_2}$]$^{10+}$. For clarity, the enantiomers of these species are not listed, and **Ad** is represented as CPK sphere. The *iso*-butoxy side chains are replaced with hydrogen atoms to reduce the computational cost. The relative energy levels (black numbers) are provided in kcal mol^{-1}.

the strain associated with the metal complexations. In energy, biconvex-[(*P,M,P/M,P,M*)-$Ag_5\mathbf{1}_2$]$^{5+}$ lies in ca. 14 kcal mol^{-1} lower than that of biconvex-[(*P,P,P/M,M,M*)-$Ag_5\mathbf{1}_2$]$^{5+}$, but is ca. 9 kcal mol^{-1} higher than that of biconcave-[(*P,M,P/M,P,M*)-$Ag_5\mathbf{1}_2$]$^{5+}$ (Fig. 3a). Similarly, for $[Hg_5\mathbf{1}_2]^{10+}$, the energy level of the biconvex-*P,M,P/M,P,M* conformers is ca. 9 kcal mol^{-1} higher than the biconcave-*P,M,P/M,P,M* ones (Fig. 3b). By the same token, biconvex-[(*P,M,P/M,P,M*)-$Hg_5\mathbf{1}_2$]$^{10+}$ is more flat (6.9 Å in height, Supplementary Table 15), compared to biconvex-[(*P,M,P/M,P,M*)-$Ag_5\mathbf{1}_2$]$^{5+}$ (height = 9.1 Å).

To further confirm the formation of the cages, more experiments were carried out. ^{1}H NMR titration of Ag(OTf) to **1** in 5:95 (v/v) $CD_3CN/CDCl_3$ clearly showed that, upon the addition of Ag^+ cations, the signals of ligands gradually became weaker, and a new set of signals corresponding to the cages appeared (Fig. 4a and Supplementary Figs. 3 and 18, 19, SI). Based on the results of DFT calculations, it is reasonable to assign this new set of signals to the racemic [biconcave-(*P,M,P*)/(*M,P,M*)-$Ag_5\mathbf{1}_2$]·$[OTf]_5$. The complexation induced significant upfield shifts of the protons, which are supposed to be located in the inner cavity, such as H_a, H_b, and H_g, as ascribed to the strong shielding of the cage (Fig. 4a). In particular, as an important indicator for the formation of cages, the methylene protons H_i on the *iso*butyl side chains split into two sets upon complexation, which results from the inequivalence between the proton directed inward and outward of the cage[70]. Additional evidence for the formation of cage complexes was also provided by the electrospray ionization—high-resolution mass spectrometry (ESI-HRMS) spectrum (Supplementary Fig. 31 and Supplementary Table 5), in which a series of prominent signals assignable to $[Ag_m\mathbf{1}_2\cdot(OTf)_n]^{m-n}$ ($m \le 5$) can be clearly observed. 2D diffusion ordered spectroscopy (DOSY) spectrum indicated the formation of a single product with a diffusion coefficient of $D = (1.42 \pm 0.01) \times 10^{-10}$ m^2 s^{-1}, which is much smaller than that of the ligand in the same solvent ($D = (3.76 \pm 0.05) \times 10^{-10}$ m^2 s^{-1}) (Supplementary Method 7, Supplementary Figs. 24−27 and Supplementary Table 4).

Except 5:95 (v/v) $CD_3CN/CDCl_3$ (dielectric constant, $\varepsilon \approx 6.4$), other three kinds of solvents, including acetone-d_6 ($\varepsilon = 21$), CD_3CN ($\varepsilon = 37$), and 1,1,2,2-tetrachloroethane-d_2 ($CDCl_2CDCl_2$, $\varepsilon = 8.5$) were also investigated. The $\mathbf{Ag_5L_2}$ cages exhibited well-resolved ^{1}H NMR spectra in acetone-d_6 and $CDCl_2CDCl_2$ (Fig. 4b and Supplementary Fig. 4d); nevertheless, in CD_3CN, broadened, overlapped signals were observed, which is probably due to the aggregation of the cages in this solvent (Supplementary Fig. 4a).

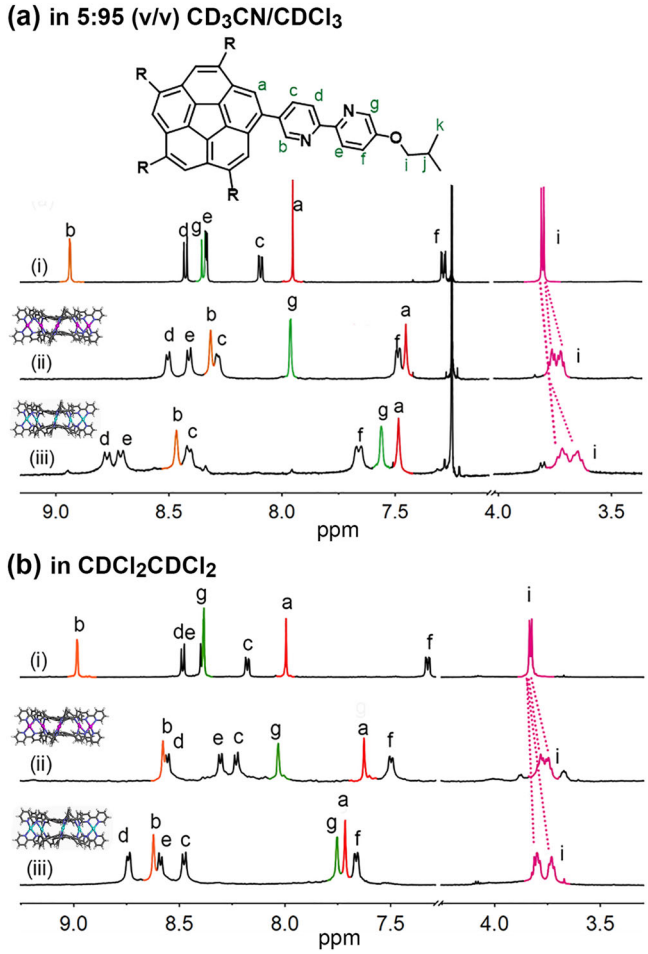

Fig. 4 | Coordination-driven self-assemblies of the Ag(I)/Hg(II) molecular cages. a ^{1}H NMR spectra of (i) the ligand (**1**), (ii) $[Ag_5\mathbf{1}_2]\cdot[OTf]_5$ (**Ag_5L_2**) and (iii) $[Hg_5\mathbf{1}_2]\cdot[OTf]_{10}$ (**Hg_5L_2**) in 5:95 (v/v) $CD_3CN/CDCl_3$. **b** ^{1}H NMR spectra of (i) the ligand (**1**), (ii) $[Ag_5\mathbf{1}_2]\cdot[OTf]_5$ (**Ag_5L_2**) and (iii) $[Hg_5\mathbf{1}_2]\cdot[OTf]_{10}$ (**Hg_5L_2**) in $CDCl_2CDCl_2$. The formations of cages give significant upfield shifts of those protons located in the inner cavity, including H_a, H_b and H_g, and a split of the H_i signals, compared to the ligand **1**.

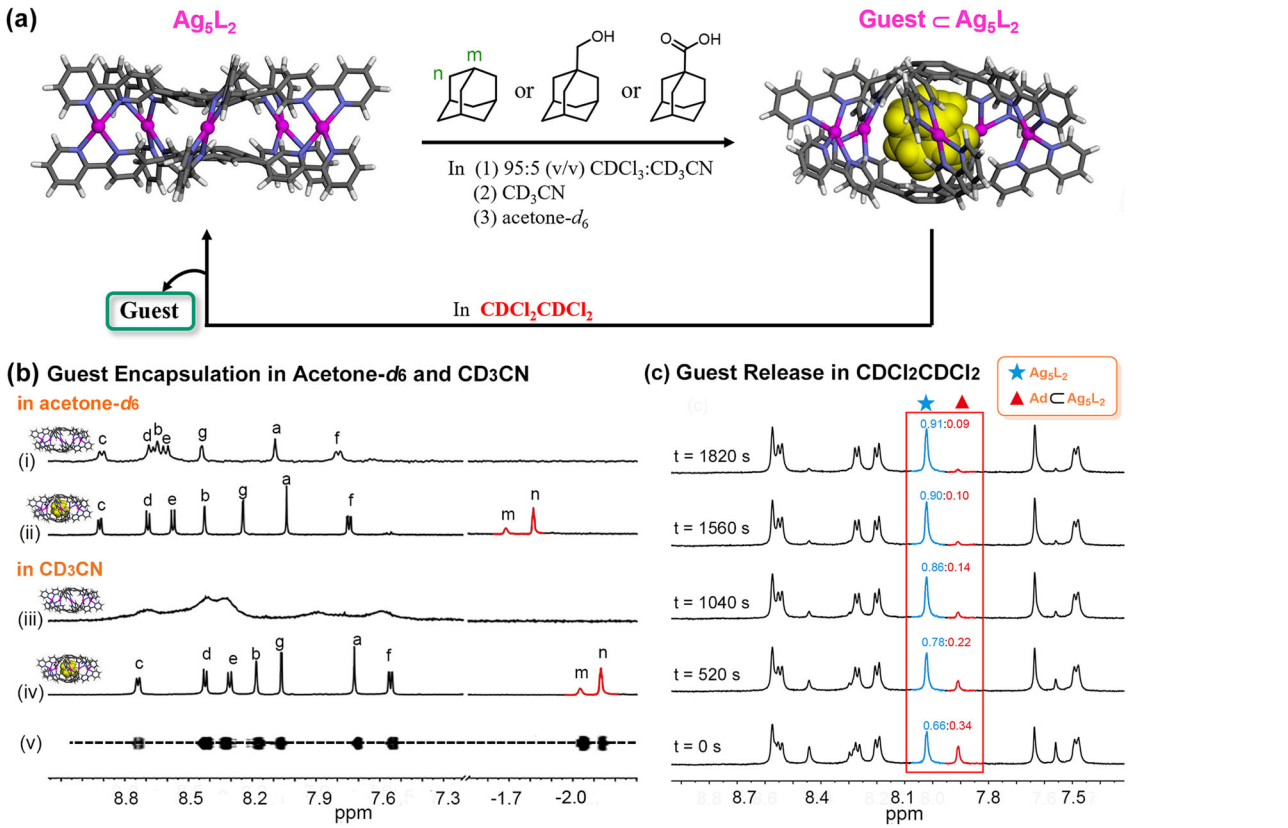

Fig. 5 | Solvent-dependent guest encapsulation and release from Ag_5L_2 cages. a A schematic representation of the host–guest chemistry of Ag_5L_2 in different solvents or solvent mixture. Ag_5L_2 can encapsulate the studied guests in 5:95 (v/v) CD_3CN/$CDCl_3$, CD_3CN and acetone-d_6. However, in $CDCl_2CDCl_2$, the included guests are gradually released from the host–guest complexes. **b** ^{1}H NMR spectrum (600 MHz, 298 K, 1 mM) of (i) Ag_5L_2 and (ii) **Ad**⊂Ag_5L_2 in acetone-d_6 as well as that of (iii) Ag_5L_2, (iv) **Ad**⊂Ag_5L_2 in CD_3CN. The DOSY spectrum (v) of **Ad**⊂Ag_5L_2 in CD_3CN showed that all signals from **Ad** with Ag_5L_2 were bound to diffuse at the same rate. **c**, Time-dependent ^{1}H NMR spectra (600 MHz, 301 K) of the mixture of Ag_5L_2 and **Ad**⊂Ag_5L_2 in $CDCl_2CDCl_2$. For experimental details, see Supplementary Method 8, SI.

For the construction of the Hg^{2+} cages, initially, we found that the titration of $Hg(OTf)_2$ to **1** gave very messy spectra. Nevertheless, adding 2.5 equiv. of the Hg^{2+} cations in a whole produced a distinct new set of signals, which can be assigned to biconcave-[(*P,M,P/M,P,M*)-$Hg_5\mathbf{1}_2$]·$[OTf]_{10}$ according to the results of DTF calculations, in all the cases of 5:95 (v/v) $CD_3CN/CDCl_3$, CD_3CN, acetone-d_6, and $CDCl_2CDCl_2$ (Fig. 4 and Supplementary Figs. 53 and 54). The formations of the Hg^{2+} cage are well confirmed by the split of H_i signal in the ^{1}H NMR spectra as well as the corresponding HRMS (Supplementary Fig. 93 and Supplementary Table 12) and 2D NMR spectra (Supplementary Figs. 83–86 and 91).

Solvent-dependent guest encapsulation and release from Ag_5L_2

Since no valuable results can be obtained from our isothermal titration calorimetry (ITC) experiments, the binding behaviour of the cages was investigated by ^{1}H NMR spectroscopy at 298 K. Considering the concave surface of corannulene, three kinds of molecules, including pseudo-spherical adamantane (**Ad**) and two of its derivatives, namely, 1-adamantanemethanol (**Ad-MeOH**) and 1-adamantanecarboxylic acid (**Ad-COOH**), was chosen as the guests in the studies.

The guests competed successfully (but laboriously) for the inner space of Ag_5L_2 with the solvent molecules in 5:95 (v/v) $CD_3CN/CDCl_3$. For example, titration of **Ad** to Ag_5L_2 produced an obvious attenuation of the signals of the cages and, meanwhile, the appearance and gradual enhancement of a new set of signals corresponding to the stable host–guest complexes (Supplementary Method 4 and Supplementary Fig. 5). A 1:1 encapsulation is strongly suggested by the ESI-HRMS of the cage-guest complexes (Supplementary Fig. 32 and Supplementary Table 5); and the DTF calculations showed that the cage can accommodate only one guest molecule as well (Fig. 3a and Supplementary Table 16). ^{1}H NMR titration of **Ad-MeOH** or **Ad-COOH** gave very similar results (Supplementary Figs. 6, 7, 33, 34 and Supplementary Table 5). Notably, the DFT calculations predicted **Ad**⊂[biconvex-(*P,M,P*)/(*M,P,M*)-$\mathbf{Ag_5L_2}$]$^{5+}$ complexes of 15 kcal mol^{-1} lower in energy in the gas phase (Fig. 3a), compared to that of **Ad**⊂[biconvex-(*P,P,P*)/(*M,M,M*)-$\mathbf{Ag_5L_2}$]$^{5+}$ ones, and a cage collapse for biconcave-[(*P,M,P/M,P,M*)-$Ag_5\mathbf{1}_2$]$^{5+}$ with **Ad** included due to their too small cavities, such that the cages might adopt biconvex-*P,M,P/M,P,M* conformations upon the guest complexations.

In acetone-d_6, addition of the studied guests to Ag_5L_2 resulted in also the guest inclusions as observed in the ^{1}H NMR spectra (Fig. 5b, Supplementary Method 5 and Supplementary Figs. 8—10). The signals of the host–guest complexes are pretty dispersed, thus being assignable, providing a good chance to explore the encapsulation behaviors. A closer examination of the ^{1}H NMR spectra indicated that the complexation induced obvious changes in chemical shift for the protons that are supposed to be located in the inner cavity, i.e., H_a and H_b, which is due to the σ—π interaction between the encapsulated guest and the host. The encapsulated guests experience a highly shielded nano-environment, thus showing one set of signals in the range of (–1.5–(–2.0)) ppm) (Fig. 5b). The encapsulation was unambiguously verified further by the 2D NOESY spectrum, which exhibited strong correlations between the protons of **Ad** and H_a/H_c of the cages (Supplementary Figs. 20–23). Interestingly, in the ^{1}H NMR spectra, the protons that are supposed to stay far from the encapsulated molecules, including H_e, H_f and H_g, also shifted to some extent, which is probably caused by a slight deformation of the cage upon guest encapsulations. In fact, the encapsulation-induced expansion was supported by the DFT calculations, which predicted a height of 10.0 Å for the energy-minimized structure of

Table 1 | Association constants (K_a, M^{-1}) and rate (k, s^{-1}) of release of various guests from Ag_5L_2 in different solvents at 298 K

Guest	Encapsulation			Release
	CD_3CN	95:5 (v/v) $CDCl_3$:CD_3CN	Acetone-d_6	$CDCl_2CDCl_2$
	K_a (M^{-1})	K_a (M^{-1})	K_a (M^{-1})	k (s^{-1})[a]
	$(1.2 \pm 0.1) \times 10^3$	23.4 ± 3.2	$(2.1 \pm 0.8) \times 10^3$	5.1×10^{-4}
	$(1.4 \pm 0.2) \times 10^4$	21.7 ± 1.6	$(6.8 \pm 1.5) \times 10^3$	2.0×10^{-3}
	$(8.9 \pm 0.5) \times 10^3$	22.3 ± 4.7	$(9.1 \pm 2.5) \times 10^2$	4.4×10^{-4}

[a]The kinetic data at 298 K are calculated by the linear extrapolation method[77]. For more parameters, see Tables S7, SI.

Ad⊂biconvex-[(*P,M,P*)/(*M,P,M*)-Ag_5L_2]$^{5+}$ (Supplementary Tables 15, 16), a little larger than that of the free cages (ca. 9.1 Å).

Ag_5L_2 includes the studied guests in CD_3CN as well. This is indicated by the appearance of a set of well-resolved signals in the ^{1}H NMR titration experiments, despite the cage itself cannot show distinct signals in such a solvent (Fig. 5biii–iv, Supplementary Method 6 and Supplementary Figs. 11–13). In addition, the DOSY spectrum showed all signals from **Ag_5L_2** and **Ad** diffusing at the same rate (Fig. 5bv and Supplementary Figs. 28, 29).

Though the ^{1}H NMR signals of the cage-guest complexes in 5:95 (v/v) CD_3CN/$CDCl_3$ are not assignable due to the weak host–guest association (giving the coexist of **Ad**⊂**Ag_5L_2** and **Ag_5L_2**) and the aggregation of the signals themselves, the molar ratio (χ) of **Ad**⊂**Ag_5L_2** against **Ag_5L_2** can still be derived from the integrations of the signals corresponding to the free cage and the cage-guest complex (Supplementary Methods 4 and Supplementary Table 1), which provided further the association constant (K_a) of 23.4 ± 3.2 M^{-1}, 21.7 ± 1.6 M^{-1} and 23.1 ± 6.5 M^{-1} for **Ad, Ad-MeOH**, and **Ad-COOH**, respectively (Table 1). The association constants in acetone-d_6 and CD_3CN can be determined in a similar manner (Supplementary Methods 5, 6 and Supplementary Tables 2, 3). Besides, compared to the case of 5:95 (v/v) CD_3CN/$CDCl_3$, the cage has ~3 orders of magnitude greater affinity for each guest in acetone-d_6, and it is enhanced further when changing the solvent to CD_3CN (Table 1). Nevertheless, in each particular solvent, the association constant is close to one other for different guests, as a comprehensive result of the interactions between the guests and the coordination cages as well as the solvents. Notably, overall, the guest-binding affinities are higher in more polar solvents. This could be first ascribed to a weaker competition from the solvent molecules for the guests with respect to host binding. Besides, in the cases of **Ad-COOH** and **Ad-OH**, looser ion-pairs between $[Ag_5\mathbf{1}_2]^{5+}$ and the counter anions (OTf^-) present in such situations, which is greatly conducive to the electrostatic interactions between the constituent metal cations and the included guests.

In contrast to those in the solvents mentioned above, **Ag_5L_2** showed much different binding behavior in $CDCl_2CDCl_2$. In such a solvent, addition of the studied guests to **Ag_5L_2** gave no changes in the ^{1}H NMR spectrum. Moreover, when the samples of guest⊂**Ag_5L_2** complexes prepared in CD_3CN were dried under vacuum and then re-dissolved in $CDCl_2CDCl_2$, with increasing the standing time, at room temperature, the ^{1}H NMR signals of the cage-guest complexes became (fast or gradually) weaker, along with the appearance of a new set of signals corresponding to the free cages, indicating that the encapsulated guests were expelled by the solvent molecules in such cases. The release processes were then monitored by ^{1}H NMR spectroscopy at various temperatures, in which the range of temperature investigated (301−208 K, 292−279 K, and 288−274 K for **Ad, Ad-MeOH** and **Ad-COOH**, respectively) was carefully chosen to give the changes measurable at reasonable time scales (Supplementary Method 8 and Supplementary Figs. 35−52). First-order rate constants, k, for the release, were obtained by monitoring the decay of the signals of the cage-guest complexes and the thriving of the free cages (Supplementary Tables 8–10). Using the rate constants obtained, the enthalpic ($\Delta H^{\ddagger}$) and entropic ($\Delta S^{\ddagger}$) contributions to the transition state were calculated from Eyring plots (Supplementary Table 6). Other kinetic parameters at 298 K were next calculated using a linear extrapolation method (Supplementary Table 7)[77].

The results show that the release rates in $CDCl_2CDCl_2$ follow the order of **Ad-MeOH** > **Ad** > **Ad-COOH**, but are basically of the same order of magnitude (Table 1). In all cases, the formation of activated complexes (the transition state) is an exothermic process (Supplementary Table 7). In the transition states, the inner cavity of the cage should be crowded with the studied guest and solvent molecules. The cage therefore needs energy to adjust itself to overcome the steric hindrance of the molecules inside. Compared to the other two kinds of guests, passing through the transition state in the case of **Ad-COOH** is less enthalpically but more entropically favored. This is probably due to the self-association of **Ad-COOH** in $CDCl_2CDCl_2$, which is a process associated with exotherm and an entropic reduction.

Solvent-independent guest encapsulation in Hg_5L_2

With the data indicative of a solvent-controlled guest binding and release from cage **Ag_5L_2** in hand, we next set out to study the binding behaviors of **Hg_5L_2**. Considering that the DFT calculations predicted a smaller height for the cavity of biconvex-[(*P,M,P*/*M,P,M*)-$Hg_5\mathbf{1}_2$]$^{10+}$ compared to biconvex-[(*P,M,P*/*M,P,M*)-$Ag_5\mathbf{1}_2$]$^{5+}$, we expected that the Hg^{2+} cage could bind the studied guests in a different manner.

DFT calculations provide a predictive insight into the encapsulation in **Hg_5L_2**, which showed that the inner cavity of biconcave-*P,M,P*/*M,P,M* are too small to accommodate **Ad** (inclusion of the guest will give a disassembly of the cage) so that only **Ad**⊂biconvex-[(*P,M,P*)/(*M,P,M*)-$Hg_5\mathbf{1}_2$]$^{10+}$ can be formed (Fig. 3b). The guest encapsulations lead to a larger deformation in the cage structure compared to that in the case of **Ag_5L_2**, particularly regarding the expansion of the inner cavity (from 6.9 Å for **Hg_5L_2** to 9.5 Å for **Ad** ⊂**Hg_5L_2** in height, compared to that from 9.1 Å for **Ag_5L_2** to 10.0 Å for **Ad**⊂**Ag_5L_2**, Supplementary Table 15).

Experimentally, encapsulations of the guests with **Hg_5L_2** are kinetically much harder than those in the cases of **Ag_5L_2** as expected (Supplementary Method 9). In all the studied solvents, directly adding the studied guests to **Hg_5L_2** at ambient temperature gave no changes in the ^{1}H NMR spectra, suggestive of higher encapsulation energy barriers. We thus tried different procedures to achieve the encapsulations.

Overall, the encapsulation barriers in CD_3CN and in acetone-d_6 is apparently similar to each other. Two procedures (labeled **Procedure A** and **B**, Supplementary Method 10) were utilized to prepare the cage-guest complexes in such cases. In **Procedure A** (from Cages to Cage-guest Complexes), to the ligand in CD_3CN (or acetone-d_6), 2.5 equiv. of Hg^{2+} cations and the guests were added in sequence, and the obtained samples were sonicated for 30 min at ambient temperature. In **Procedure B** (One-Pot Construction), the mixtures of the ligand and the guest in CD_3CN (or acetone-d_6) were added 2.5 equiv. of Hg^{2+} cations, followed by a sonication at ambient temperature. Both procedures resulted in the same outcomes. In the ^{1}H NMR spectra, the guest encapsulations gave rise to the disappearance of the cage signals and the presence of the new ones corresponding to the host–guest complexes (Supplementary Figs. 6b, 55–60, 87–90, 92, and 94 and Supplementary Table 13). Particularly, distinct resonances from the encapsulated guests in the inner cavity can be clearly observed in a high-field region of −1.0 ~−3.0 ppm.

In 5:95 (v/v) CD_3CN/$CDCl_3$, it is hard to produce the cage-guest complexes by sonicating the mixtures of the cage and the guests, or the mixtures of the ligand, Hg^{2+} cations and the guests, at ambient temperature. Nevertheless, by heating the mixtures of the cage and the guests at 50 °C for 2–3 days (**Procedure C**, Supplementary Method 11), the desired encapsulations can still be achieved (Supplementary Fig. 61). Alternatively, the

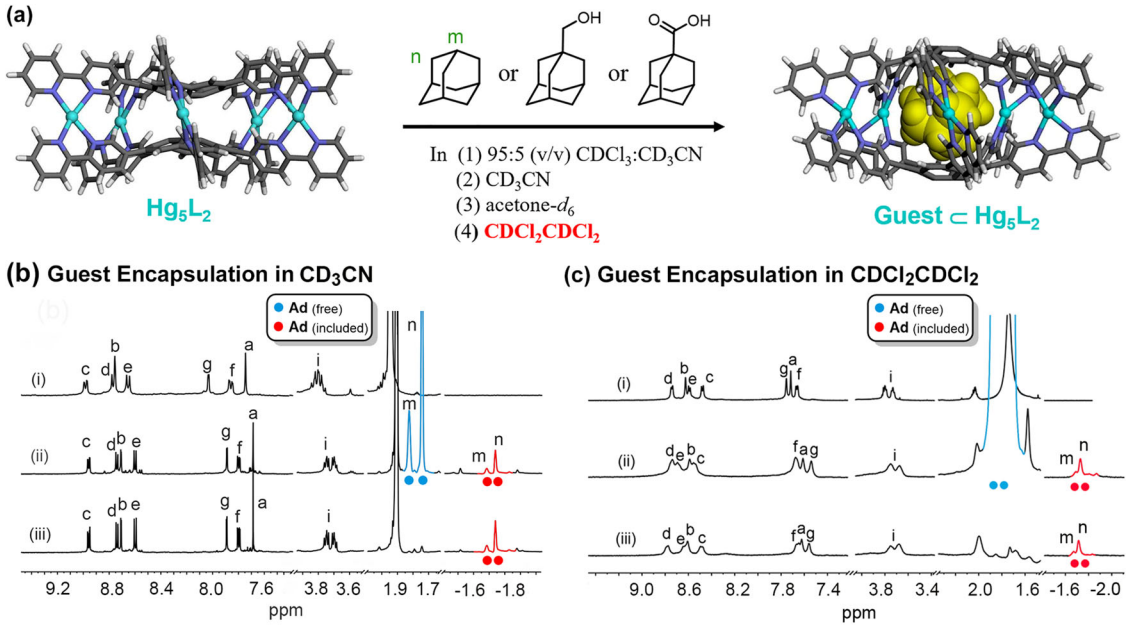

Fig. 6 | Solvent-independent guest encapsulation in the Ag_5L_2 cage. a Schematic representation of the host–guest chemistry of Hg_5L_2 in different solvents or solvent mixture. In all the studied solvent systems, including $CDCl_2CDCl_2$, the Hg_5L_2 cages can encapsulate the guests to form stable host–guest complexes. **b** ^{1}H NMR spectra (600 MHz, 298 K, 1 mM, CD_3CN) of (i) Hg_5L_2, (ii) **Ad**⊂Hg_5L_2 in the presence of 8 equiv. of **Ad** (prepared via **Procedure A**), and (iii) **Ad**⊂Hg_5L_2 in the absence of free **Ad** after the solution was stored at 298 K for 2 days. **c** ^{1}H NMR spectra (600 MHz, 298 K, 1 mM $CDCl_2CDCl_2$) of (i) Hg_5L_2, (ii) **Ad**⊂Hg_5L_2 in the presence of 200 equiv. of **Ad** (prepared via **Procedure E**), and (iii) **Ad**⊂Hg_5L_2 in the absence of free **Ad** after the solution was kept at 298 K for 2 days. For experimental details, see Methods.

complexes can be first prepared in CD_3CN or acetone-d_6, followed the replacement of the solvent with 5:95 (v/v) $CD_3CN/CDCl_3$ (**Procedure D**, Solvent-replacement Method, Supplementary Method 11 and Supplementary Figs. 62–64).

With $CDCl_2CDCl_2$ as the solvent, the encapsulations are even harder, which cannot be achieved via **Procedure C**. However, taking **Ad** as an example, when heating the mixtures of the cage and a large excess of the guest (200 equiv.) at 90 °C for 6 days, the cages underwent a complete transformation to the cage–guest complexes (**Procedure E**, Fig. 6c, Supplementary Method 12) (Supplementary Fig. 65). The same result can be obtained by heating the mixtures of the ligand, Hg^{2+} cations and the guests at 90 °C for 3 days (**Procedure F**, Supplementary Method 12) (Supplementary Figs. 66 and 67). Nevertheless, the simplest way to prepare the cage-guest complexes in such a situation still points to **Procedure D**, except that the solvent, CD_3CN or acetone-d_6, was finally replaced by $CDCl_2CDCl_2$ after the accomplishment of the guest encapsulations (Supplementary Method 11) (Supplementary Figs. 68−70).

We next assessed the stabilities of the Hg_5L_2-guest complexes in the studied solvents (or solvent mixture) at room temperature. In the investigations, the Hg_5L_2-guest complexes were first prepared in acetone-d_6 according to **Procedure A** and then dried. Since a large amount of guest was used in the procedure, to get a clear observation on the possible release of the guests as well as to avoid the possible exchange of the guest molecules between inside and outside of the cage cavity, the free guests in the obtained solid mixtures were next removed completely by solvent-washing using cyclohexane. After the pure cage-guest complexes were re-dissolved in the studied solvents (or solvent mixture), decays of the complexes were monitored at 25 °C by ^{1}H NMR spectroscopy for 2 days, and the stabilities of the complexes were assessed according to whether the signals of the free cages and the free guests reappear in the spectra (Methods, the main text).

The results show that, in all the studied solvents, particularly in the cases of $CDCl_2CDCl_2$, no included guest molecules were expelled from the cages (Fig. 6b, c Supplementary Table 11 and Supplementary Figs. 71–82). This is very interesting because such results are unambiguously indicative of a solvent-independent guest encapsulation for the Hg^{2+} cages in the studied cases (Fig. 6a).

Ag_5L_2 ⇆ Hg_5L_2 conversions

Transmetallations have been proven to be an effective way to achieve guest release from cages, as we mentioned above[40]. Given that the main difference in guest encapsulation between Ag_5L_2 and Hg_5L_2 is shown in $CDCl_2CDCl_2$, we then set about investigating the possibility of the interconversion of Ag_5L_2 ⇆ Hg_5L_2 in $CDCl_2CDCl_2$ (Fig. 7a).

The strength of the association between Hg^{2+} cations and ligand **1** is much larger than that for Ag^+ ones. Therefore, the conversion from Ag_5L_2 to Hg_5L_2 can be readily achieved by adding the Hg^{2+} cations to the solution of Ag_5L_2, as evidenced by the reappearance of Hg_5L_2 signals in the ^{1}H NMR spectrum (Fig. 7b, Supplementary Method 14 and Supplementary Fig. 97). Comparatively, the conversion from Hg_5L_2 to Ag_5L_2 is much more complicated in methodology. Our attempts in this regard were baffled for a long time until we were drawn to the function of EDTA as the competitive chelating agent. EDTA can form very stable complexes with most metal cations. In particular, in water at 25 °C, the stability constant of Hg^{2+}-EDTA (**HgEDTA**) complexes is ca. 14 orders of magnitude higher than that of Ag^+-EDTA (**AgEDTA**) ($\log K = 21.6$ and 7.2 in the case of Hg^{2+} and Ag^+, respectively)[78]. We thus tried to use the Ag^+ cations in **AgEDTA** to displace the Hg^{2+} ones in Hg_5L_2.

In our experiment, an aqueous solution of **AgEDTA** was first prepared by mixing Na_2EDTA and 1.5 equiv. of $AgNO_3$ in water. The solution was transferred to a vial containing a solution of Hg_5L_2 in $CDCl_2CDCl_2$ and the obtained bilayer mixture was vigorously stirred at 28 °C. To monitor the ion-exchange process, a series of samples taken regularly from the mixture and washed with water was characterized by ^{1}H NMR spectroscopy (Supplementary Method 13). As shown in Fig. 7c and Supplementary Fig. 95, as expected, the metal cation-exchanges occurred on the water-$CDCl_2CDCl_2$ interface, giving rise to an immediate disappearance of the signals of Hg_5L_2 in the organic phase and, finally (ca. 40 min later), the only one set of district signals corresponding to Ag_5L_2. The exchanges process should be a non-synergistic one: A stepwise ion-exchange is strongly suggested by the loss of

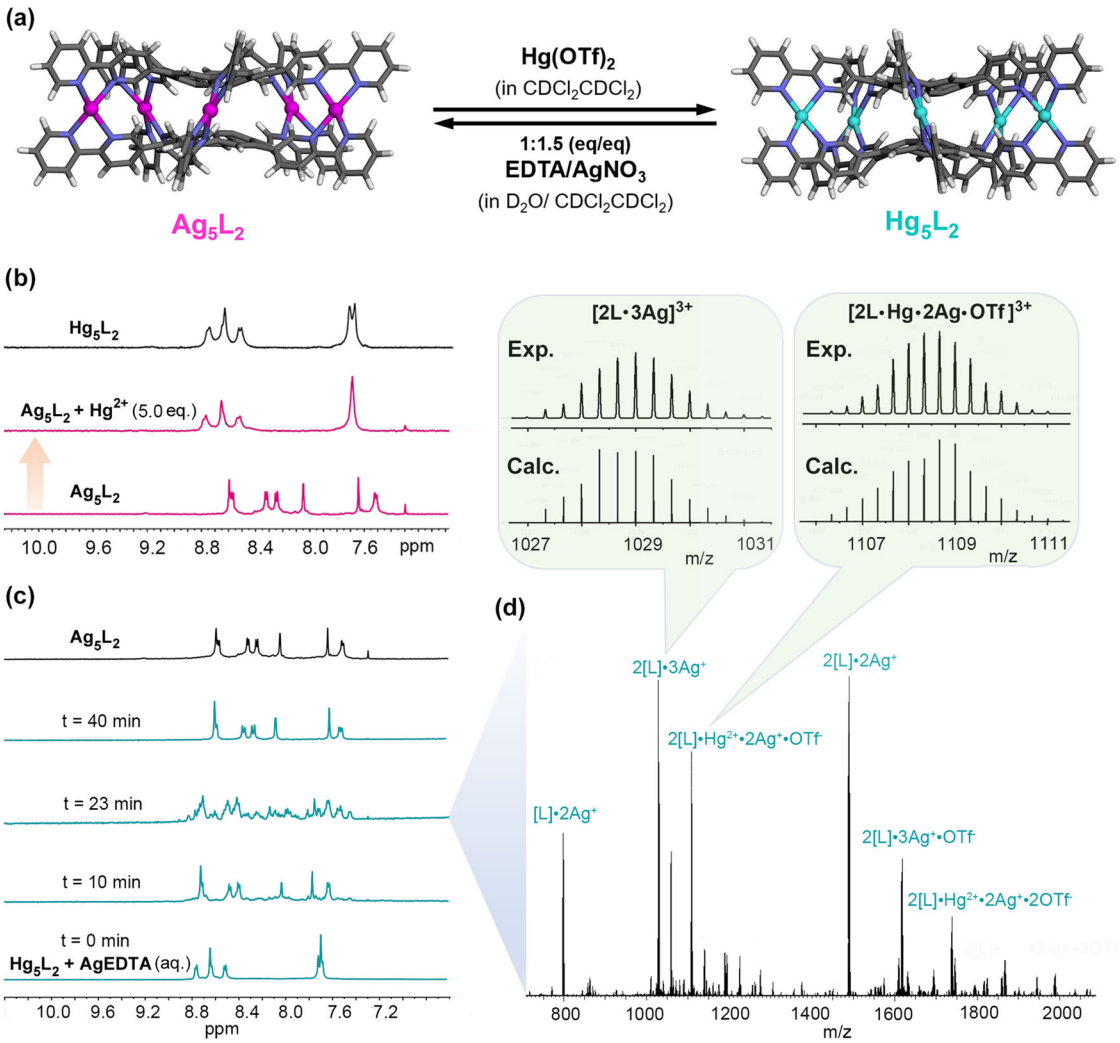

Fig. 7 | Interconversions between Ag_5L_2 and Hg_5L_2. a Schematic representation of the transmetallation-guided interconversions. **b** ^{1}H NMR spectra (600 MHz, 298 K, $CDCl_2CDCl_2$) of $\mathbf{Ag_5L_2}$ and $\mathbf{Ag_5L_2}$ in the presence of 5.0 equiv. of Hg^{2+} cation. The latter produced a solution of $\mathbf{Hg_5L_2}$ immediately due to a much stronger association strength with ligand **1** for the Hg^{2+} cations. For comparison, the spectrum of $\mathbf{Hg_5L_2}$ in $CDCl_2CDCl_2$ is shown. **c** Stacked plots of the time-depended ^{1}H NMR spectra (600 MHz, 298 K, $CDCl_2CDCl_2$) of the organic phase of the mixture of $\mathbf{Hg_5L_2}$ in $CDCl_2CDCl_2$ and an aqueous solution of **AgEDTA** under vigorous stirring at 28 °C. The metal cation exchanges that occurred on the water-$CDCl_2CDCl_2$ interface gave rise to a formation of $\mathbf{Ag_5L_2}$ finally. The spectrum of $\mathbf{Ag_5L_2}$ in $CDCl_2CDCl_2$ is shown for comparison. **d** The corresponding ESI-MS spectrum of the sample at $t = 23$ min. The insets show the experimental and simulated isotopic clusters for two intermediate species, $[2\,L{\bullet}3Ag]^{3+}$ and $[2\,L{\bullet}Hg{\bullet}3Ag{\bullet}OTf]^{3+}$.

C_5-symmetry for the cage in the ^{1}H NMR spectrum (can be clearly observed at $t = 23$ and 27 min, Fig. 7c and Supplementary Fig. 95B); and the intermediates, in which the two types of metal ions (Ag^+ and Hg^{2+}) were coordinated to form heterometallic cages, were evidenced by the HR ESI-MS of the sample $t = 23$ min (Fig. 7d, Supplementary Fig. 96 and Supplementary Table 14), which showed a series of intense peaks assignable to mixed-metal cages with different stoichiometries for the composition of cooridnated Ag^+ and Hg^{2+} cations.

Metal-cation-and-solvent-gated guest release

We finally explored the possibility of the conversion from $\mathbf{Hg_5L_2}$ to $\mathbf{Ag_5L_2}$ with the guests included (Fig. 8a). Based on the binding properties of $\mathbf{Ag_5L_2}$, in $CDCl_2CDCl_2$, such conversion means theoretically a complete guest release from the cages after the obtained mixture is stored at room temperature for, at most, a couple of hours (Supplementary Table 6).

Experimentally, the samples of guest⊂$\mathbf{Hg_5L_2}$ complexes in acetone-d_6 were first prepared according to **Procedure A**. The free guests were removed, and the solvent was changed to $CDCl_2CDCl_2$, followed by the same transmetallation procedure (Fig. 8b) as that for the conversion from $\mathbf{Hg_5L_2}$ to $\mathbf{Ag_5L_2}$ in the absence of guests. A series of samples were taken regularly from the vigorously stirring mixture of $\mathbf{Hg_5L_2}$ in $CDCl_2CDCl_2$ and aqueous **AgEDTA**. The organic-phase solutions of these samples were washed with water immediately, followed characterizations via ^{1}H NMR spectroscopy (Methods, the main text).

Basically, two series of spectra were obtained in each case. The first series of spectra (Supplementary Figs. 98, 100, and 102) were recorded soon after the samples were sucked out of the bilayer mixture and washed with water, which was used to detect the species in the organic-phase solution of the stirring bilayer mixture; and another series of spectra (Fig. 8c, Supplementary Figs. 99, 101, and 103) were recorded after these samples were stored further at 28 °C for 4 h (to get fully released for the guests).

The results showed that the cation-exchanges indeed occurred in the vigorously stirring mixture to give guest⊂$\mathbf{Ag_5L_2}$ complexes. However, we were surprised to observe that it was more difficult to liberate the included guests from $\mathbf{Ag_5L_2}$ cages in the stirring bilayer mixtures (Supplementary Figs. 98, 100, and 102), compared to those in the cases of guest⊂$\mathbf{Ag_5L_2}$ in pure $CDCl_2CDCl_2$ (Supplementary Table 6 and 7). Taking the case of **Ad** as an example, strong signals of the included **Ad** can still be observed in the ^{1}H

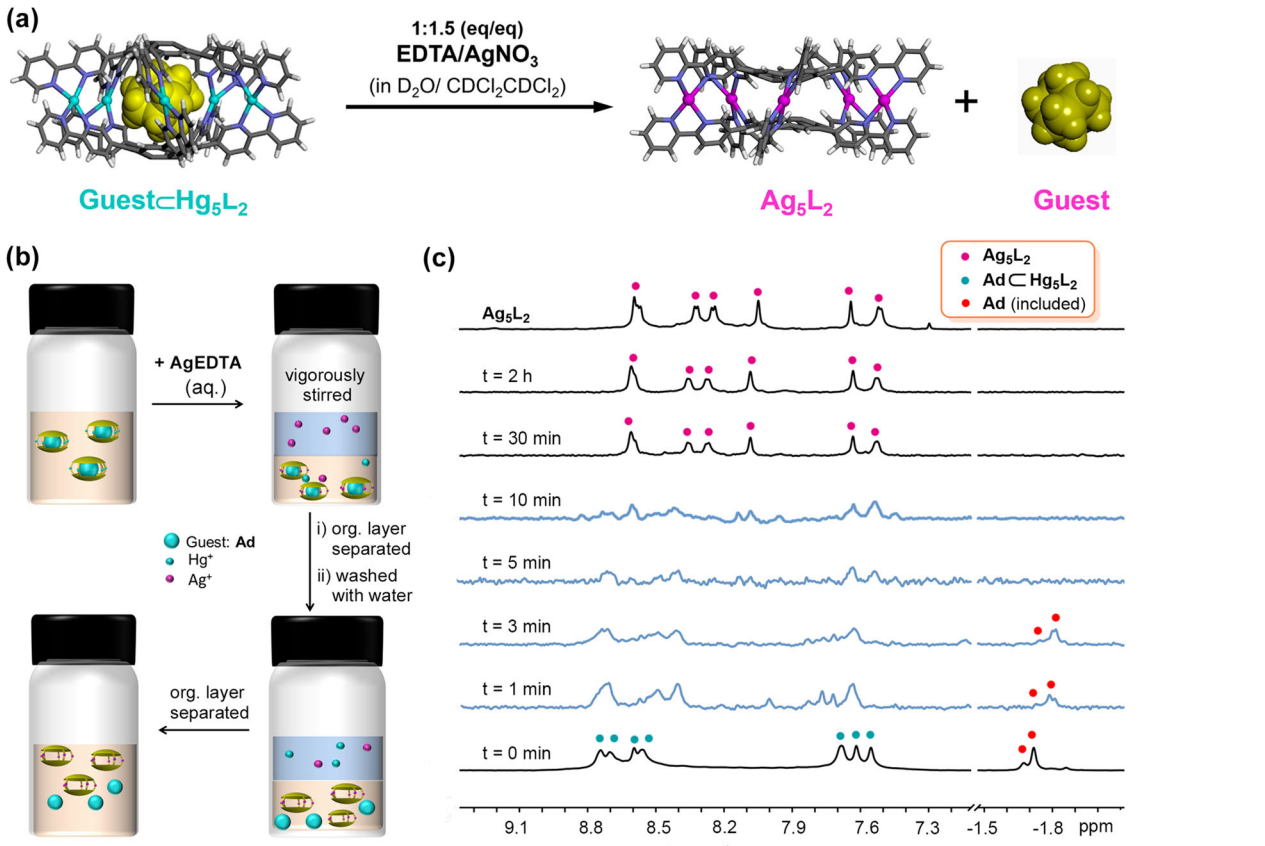

Fig. 8 | Metal-cation-and-solvent-controlled guest release from Hg_5L_2. **a** Schematic showing the metal cation-guided guest release from Hg_5L_2 in $CDCl_2CDCl_2$. **b** Cartoon representation of the protocol operation for releasing **Ad** from **Ad⊂Hg_5L_2** complexes. Initially, an aqueous solution of **AgEDTA** was added to Hg_5L_2 in $CDCl_2CDCl_2$. The bilayer mixture was vigorously stirred at 28 °C. Samples were taken regularly from the mixture and the organic phase was separated and washed with water. The resulting solutions were further stored at 28 °C for 4 h before being characterized by ^{1}H NMR spectroscopy which gave (**c**) a series of ^{1}H NMR spectra (600 MHz, 298 K, $CDCl_2CDCl_2$) tracking the cage transformation and the guest release over time. The stirring time on the bilayer mixture of **Ad⊂Hg_5L_2** and **AgEDTA** (aq.) is provided in minutes in Fig. 8c.

NMR spectrum even the mixture was stirred for 2 h (Supplementary Fig. 98A). This is probably due to the presence of **HgEDTA** in the systems, binding exohedrally to the silver cages thus hindering the release of the guests. Nevertheless, for the samples those were washed with water (**HgEDTA** removed) and then stored for 4 h, no signals of the included **Ad** were observable, as long as the mixture of **Ad⊂Hg_5L_2/AgEDTA** was stirred at 28 °C for no <5 min (t = 5–120 min, Fig. 8c and Supplementary Fig. 99), indicative of a complete **Ad** release from the silver cages in these cases. Notably, it seems that **Ad** can even be released from some heterometallic cages, given that, at t = 5 or 10 min, the Hg^{2+} cations in the cages have not been completely replaced by the Ag^+ ones (Fig. 8c and Supplementary Fig. 99). Similar phenomena were also observed in the cases of **Ad-MeOH** and **Ad-COOH** (Supplementary Figs. 101 and 103). All these demonstrate that the release of the guests from Hg_5L_2 can be synergistically controlled by metal cations and solvents.

Conclusion

In summary, we have demonstrated the synthesis, characterization and host–guest chemistry of two 1,3,5,7,9-penta(2,2'-bipyridin-5-yl)corannulene-based coordination cages, Hg_5L_2 and Ag_5L_2. Host–guest studies with the cages and three adamantane-based guests (**Ad, MeOH** and **Ad-COOH**) revealed that, while the former can encapsulate the guest molecules to form stable host–guest complexes in all four kinds of solvents (or solvent mixture), including acetone-d_6, CD_3CN, 5:95 (v/v) $CD_3CN/CDCl_3$ and $CDCl_2CDCl_2$, the latter shows a guest encapsulation capability in three kinds of the solvents and a guest-release behavior in $CDCl_2CDCl_2$. The two kinds of coordination cages are interconvertible. Therefore, to release the included guests from Hg_5L_2 in some solvents, such as acetone-d_6, both the solvent and the metal cations have to be changed. This thus, in fact, represents a dual-controlled guest release system, performing the task only if there are the right metal cations and, at the same time, the right solvent. Such kind of anti-interference release systems may cooperate with a single-controlled guest release system, such as Ag_5L_2 in the studied case, to find applications in programmable synthesis, in which different reactants or catalysts are sequentially released under rational stimuli.

Methods

Stability studies on guest⊂Hg_5L_2 complexes in solutions

Three kinds of complexes, including **Ad⊂**$[Hg_5\mathbf{1}_2]\cdot[OTf]_{10}$, **Ad-MeOH⊂**$[Hg_5\mathbf{1}_2]\cdot[OTf]_{10}$, and **Ad-COOH⊂**$[Hg_5\mathbf{1}_2]\cdot[OTf]_{10}$, and four different solvent systems, including (i) CD_3CN, (ii) acetone-d_6, (iii) 95:5 (v/v) $CDCl_3/CD_3CN$ and (iv) $CDCl_2CDCl_2$, were investigated. The complexes in CD_3CN and in acetone-d_6 were prepared according to **Procedure A** (Supplementary Method 10), and those in 95:5 (v/v) $CDCl_3/CD_3CN$ and in $CDCl_2CDCl_2$ were constructed via **Procedure D** (Supplementary Method 11). Since, in all the cases, the Hg_5L_2-guest complexes were prepared using much excess amount of guest compared to that of the cage, to get a clearer observation on the possible release of the guest from the cage as well as to avoid the possible change of the guest molecules between inside and outside of the cage cavity, after the cage-guest complexes were constructed, the free guest in the obtained mixture was first removed by solvent-washing. Then, decays of the complexes were monitored. Typical procedures for the construction of Hg_5L_2-guest complexes, the free-guest elimination and the stability studies are as follows.

(a) Construction of $\mathbf{Hg_5L_2}$-guest complexes and free-guest elimination. To a sample of ligand **1** (2 mM, 0.5 mL) in acetone-d_6, $Hg(OTf)_2$ (200 mM, acetone-d_6) was added to give a 1 mM $\mathbf{Hg_5L_2}$ cage solution. To this solution, 8 equivalents of guest (50 mM, acetone-d_6) was added. The mixture was sonicated at ambient temperature for 30 min, then evacuated under reduced pressure to dryness. The residue was re-dissolved in cyclohexane (4 ml) to give a turbid mixture. This mixture was sonicated at ambient temperature for 10 min and centrifuged, then the top homogenous solution was removed with a pipet. The solvent-washing procedure was repeated for total 5 times. Finally, the obtained solid was evacuated under high vacuum, and then re-dissolved into one of the studied solvents (or solvent mixture). ^{1}H NMR spectra of the solids showed that all the free-guests were removed, as evidenced by the disappearance of the free-guest signals which typically showed at $\delta = 1.4 - 2.0$ ppm (Supplementary Figs. 71A−79B and 80−82).

(b) Stability studies. The stability of the cage-guest complexes in different solvents (acetone-d_6, CD_3CN, 5:95(v/v) $CD_3CN/CDCl_3$ or $CDCl_2CDCl_2$) was measured by ^{1}H NMR spectroscopy. Decays of the complexes can be assessed according to the ratio (based on signal integrals) of the cage-guest complexes to the free cages or guests that reappeared in the spectra. The complexes in the solution were monitored for two days. The obtained spectra are shown in Supplementary Figs. 71A−79B and 80−82, which shown that no guest molecules released from the cage cavity in all the cases. The results can be expressed as shown in Supplementary Table 11.

Guest⊂$\mathbf{Hg_5L_2}$→guest + $\mathbf{Ag_5L_2}$ conversion

To ligand **1** (1 equiv), the guest (4 equiv), and $Hg(OTf)_2$ (2.5 equiv) in a vial, solvent acetone was added, and the mixture was sonicated at ambient temperature for 30 min. The obtained solution was checked by ^{1}H NMR spectroscopy at the end of the sonication to make sure that the host–guest complexes had completely formed. The solution was next transferred to a centrifuge tube, evacuated under reduced pressure to dryness. The solid residue was washed with cyclohexane (HPLC Grade). After the free guest has been confirmed to be completely removed by ^{1}H NMR spectroscopy, the host–guest complexes were further dried under high-vacuum and then re-dissolved in $CDCl_2CDCl_2$ (4 ml) to give a 1 mM solution. The solution was transferred to a vial (I.D. 25 mm, 10 ml) with a magnetic stir bar (olive shape, diameter 9 mm, length 15 mm). To this solution, an aqueous solution of (1:1.5, equiv/equiv) $Na_2EDTA/AgNO_3$ (50 mM, 4 ml) was added. The mixture was vigorously stirred (950 rpm) at 28 °C. Samples were taken regularly from the mixture, and washed immediately with brine (×3) and pure water (×2), followed by drying with sodium sulfate. The series of samples were characterized by ^{1}H NMR spectroscopy after been diluted twofold with $CDCl_2CDCl_2$.

Basically, two series of spectra were obtained for each case. The first series of spectra (Supplementary Figs. 98A, B, 100A, B and 102A, B) were recorded soon after the samples were sucked out of the bilayer mixture and washed with water, which was used to detect the species in the organic-phase solution of the stirring bilayer mixture; and another series of spectra (Fig. 8c, Supplementary Figs. 99A, B, 101A, B, and 103A, B) were recorded after these samples were stored further at 28 °C for 4 h (to get fully released for the guests). The obtained time-dependent ^{1}H NMR spectra showed that Guest⊂$[Hg_5\mathbf{1}_2]\cdot[OTf]_{10}$ has successfully turned into $[Ag_5\mathbf{1}_2]\cdot[OTf]_{10}$ with the guests released at the end of the conversion.

Data availability

All data are included in this article, Supplementary Information and Supplementary Data (NMR spectra). The data are available from the corresponding author upon reasonable request.

Received: 18 January 2024; Accepted: 9 February 2024;
Published online: 27 February 2024

References

1. Batool, S. et al. A detailed insight of the tumor targeting using nanocarrier drug delivery system. *Drug Deliv.* **30**, 2183815–2183834 (2023).
2. Slowing, I. I., Vivero-Escoto, J. L., Wu, C.-W. & Lin, V. S.-Y. Mesoporous silica nanoparticles as controlled release drug delivery and gene transfection carriers. *Adv. Drug Deliv. Rev.* **60**, 1278–1288 (2008).
3. Yu, Z. et al. Kinetics driven by hollow nanoreactors: an opportunity for cotrollable. *Catal. Angew. Chem. Int. Ed.* **62**, e202213612 (2023).
4. Dooley, C. & Taylor, D. Self-healing materials: what can nature teach us? *Fatigue Fract. Eng. Mater. Struct.* **40**, 655–669 (2017).
5. White, S. R. et al. Autonomic healing of polymer composites. *Nature* **409**, 794–797 (2001).
6. Zhang, A., Jung, K., Li, A., Liu, J. & Boyer, C. Recent advances in stimuli-responsive polymer systems for remotely controlled drug release. *Prog. Polym. Sci.* **99**, 101164–101190 (2019).
7. Zangabad, P. S. et al. Nanocaged platforms: modification, drug delivery and nanotoxicity. Opening synthetic cages to release the tiger. *Nanoscale* **9**, 1356–1392 (2017).
8. Krykun, S. et al. Metalla-assembled electron-rich tweezers: redox-controlled guest release through supramolecular dimerization. *Angew. Chem. Int. Ed.* **59**, 716–720 (2020).
9. Owh, C. et al. Bottom-up design of hydrogels for programmable drug release. *Biomater. Adv.* **141**, 213100–213115 (2022).
10. Chakrabarty, R., Mukherjee, P. S. & Stang, P. J. Supramolecular coordination: self-assembly of finite two- and three-dimensional ensembles. *Chem. Rev.* **111**, 6810–6918 (2011).
11. Ajami, D., Liu, L. & Rebek, J. Jr. Soft templates in encapsulation complexes. *Chem. Soc. Rev.,* **44**, 490–499 (2015).
12. Kawamichi, T., Haneda, T., Kawano, M. & Fujita, M. X-ray observation of a transient hemiaminal trapped in a porous network. *Nature* **461**, 633–635 (2009).
13. Mal, P., Breiner, B., Rissanen, K. & Nitschke, J. R. White phosphorus is air-stable within a self-assembled tetrahedral capsule. *Science* **324**, 1697–1699. (2009).
14. Wang, K., Jordan, J. H., Hu, X.-Y. & Wang, L. Supramolecular strategies for controlling reactivity within confined nanospaces. *Angew. Chem. Int. Ed.* **59**, 13712–13721 (2020).
15. Sun, W. et al. Self-assembled carcerand-like cage with a thermoregulated selective binding preference for purification of high-purity C_{60} and C_{70}. *J. Org. Chem.* **83**, 14667–14675 (2018).
16. Xue, W. et al. Subtle stereochemical effects influence binding and purification abilities of an $Fe^{II}_4L_4$ Cage. *J. Am. Chem. Soc.* **145**, 5570–5577 (2023).
17. Mal, P., Schultz, D., Beyeh, K., Rissanen, K. & Nitschke, J. R. An unlockable–relockable iron cage by subcomponent self-assembly. *Angew. Chem. Int. Ed.* **47**, 8297–8301 (2008).
18. Lewis, J. E. M., Gavey, E. L., Cameron, S. A. & Crowley, J. D. Stimuli-responsive Pd_2L_4 metallosupramolecular cages: towards targeted cisplatin drug delivery. *Chem. Sci.* **3**, 778–784 (2012).
19. Kishi, N., Akita, M. & Yoshizawa, M. Selective host–guest interactions of a transformable coordination capsule/tube with fullerenes. *Angew. Chem. Int. Ed.* **53**, 3604–3607 (2014).
20. Jiménez, A. et al. Selective encapsulation and sequential release of guests within a self-sorting mixture of three tetrahedral cages. *Angew. Chem. Int. Ed.* **53**, 4556–4560 (2014).
21. Croué, V., Goeb, S., Szalóki, G., Allain, M. & Sallé, M. Reversible guest uptake/release by redox-controlled assembly/disassembly of a coordination cage. *Angew. Chem. Int. Ed.* **55**, 1746–1750 (2016).
22. McConnell, A. J., Aitchison, C. M., Grommet, A. B. & Nitschke, J. R. Subcomponent exchange transforms an $Fe^{II}_4L_4$ cage from high- to low-spin, switching guest release in a two-cage system. *J. Am. Chem. Soc.* **139**, 6294–6297 (2017).
23. Jansze, S. M., Cecota, C. & Severin, K. Reversible disassembly of metallasupramolecular structures mediated by a metastable-state photoacid. *Chem. Sci.* **9**, 4253–4257 (2018).
24. Ogata, D. & Yuasa, J. Dynamic open coordination cage from nonsymmetrical imidazole–pyridine ditopic ligands for turn-on/off anion binding. *Angew. Chem. Int. Ed.* **58**, 18424–18428 (2019).

25. Xu, L., Zhang, D., Ronson, T. K. & Nitschke, J. R. Improved acid resistance of a metal–organic cage enables cargo release and exchange between hosts. *Angew. Chem. Int. Ed.* **59**, 7435–7438 (2020).
26. Lisboa, L. S., Findlay, J. A., Wright, L. J., Hartinger, C. G. & Crowley, J. D. A reduced-symmetry heterobimetallic $[PdPtL_4]^{4+}$ cage: assembly, guest binding, and stimulus-induced switching. *Angew. Chem. Int. Ed.* **59**, 11101–11107 (2020).
27. Bolliger, J. L., Ronson, T. K., Ogawa, M. & Nitschke, J. R. Solvent effects upon guest binding and dynamics of a $Fe^{II}_4L_4$ cage. *J. Am. Chem. Soc.* **136**, 14545–14553 (2014).
28. Löffler, S. et al. Triggered exchange of anionic for neutral guests inside a cationic coordination cage. *J. Am. Chem. Soc.* **137**, 1060–1063 (2015).
29. Bai, X. et al. Peripheral templation-modulated interconversion between an A_4L_6 tetrahedral anion cage and A_2L_3 triple helicate with guest capture/release. *Angew. Chem., Int. Ed.* **57**, 1851–1855 (2018).
30. Zhang, D., Ronson, T. K., Lavendomme, R. & Nitschke, J. R. Selective separation of polyaromatic hydrocarbons by phase transfer of coordination cages. *J. Am. Chem. Soc.* **141**, 18949–18953 (2019).
31. Endo, K., Ube, H. & Shionoya, M. Multi-stimuli-responsive interconversion between bowl- and capsule-shaped self-assembled Zinc(II) complexes. *J. Am. Chem. Soc.* **142**, 407–416 (2020).
32. Han, M. et al. Light-triggered guest uptake and release by a photochromic coordination cage. *Angew. Chem. Int. Ed.* **52**, 1319–1323 (2013).
33. Li, R.-J., Holstein, J. J., Hiller, W. G., Andréasson, J. & Clever, G. H. Mechanistic interplay between light switching and guest binding in photochromic [Pd_2Dithienylethene$_4$] coordination cages. *J. Am. Chem. Soc.* **141**, 2097–2103 (2019).
34. Pesce, L., Perego, C., Grommet, A. B., Klajn, R. & Pavan, G. M. Molecular factors controlling the isomerization of azobenzenes in the cavity of a flexible coordination cage. *J. Am. Chem. Soc.* **142**, 9792–9802 (2020).
35. Lee, H. et al. Light-powered dissipative assembly of diazocine coordination cages. *J. Am. Chem. Soc.* **144**, 3099–3105 (2022).
36. Ghosh, A. et al. Light-powered reversible guest release and uptake from Zn_4L_4 capsules. *J. Am. Chem. Soc.* **145**, 3828–3832 (2023).
37. Mendez-Arroyo, J., d'Aquino, A. I., Chinen, A. B., Manraj, Y. D. & Mirkin, C. A. Reversible and selective encapsulation of dextromethorphan and β-estradiol using an asymmetric molecular capsule assembled via the weak-link approach. *J. Am. Chem. Soc.* **139**, 1368–1371 (2017).
38. Djemili, R. et al. Positive allosteric control of guests encapsulation by metal binding to covalent porphyrin cages. *Chem. Eur. J.* **25**, 1481–1487 (2019).
39. Bruns, C. J. et al. Emergent ion-gated binding of cationic host–guest complexes within cationic $M_{12}L_{24}$ molecular flasks. *J. Am. Chem. Soc.* **136**, 12027–12034 (2014).
40. Gan, Q., Ronson, T. K., Vosburg, D. A., Thoburn, J. D. & Nitschke, J. R. Cooperative loading and release behavior of a metal–organic receptor. *J. Am. Chem. Soc.* **137**, 1770–1773 (2015).
41. Szalóki, G. et al. Controlling the host–guest interaction mode through a redox stimulus. *Angew. Chem. Int. Ed.* **56**, 16272–16276 (2017).
42. Lu, Z., Ronson, T. K. & Nitschke, J. R. Reversible reduction drives anion ejection and C_{60} binding within an $Fe^{II}_4L_6$ cage. *Chem. Sci.* **11**, 1097–1101 (2020).
43. Hamashima, K. & Yuasa, J. Entropy versus enthalpy controlled temperature/redox dual-triggered cages for selective anion encapsulation and release. *Angew. Chem. Int. Ed.* **61**, e202113914 (2022).
44. Ozores, H. L., Amorín, M. & Granja, J. R. Self-assembling molecular capsules based on α,γ-cyclic peptides. *J. Am. Chem. Soc.* **139**, 776–784 (2017).
45. Takata, H., Ono, K. & Iwasawa, N. Controlled release of the guest molecule via borate formation of a fluorinated boronic ester cage. *Chem. Commun.* **56**, 5613–5616 (2020).
46. Kurihara, K., Yazaki, K., Akita, M. & Yoshizawa, M. A switchable open/closed polyaromatic macrocycle that shows reversible binding of long hydrophilic molecules. *Angew. Chem. Int. Ed.* **56**, 11360–11364 (2017).
47. Zhiquan, L. et al. A stimuli-responsive molecular capsule with switchable dynamics, chirality, and encapsulation characteristics. *J. Am. Chem. Soc.* **140**, 11091–11100 (2018).
48. Zhou, L.-P., Feng, X.-S., Hu, S.-J. & Sun, Q.-F. Controlled self-assembly, isomerism, and guest uptake/release of charge-reversible lanthanide–organic octahedral cages. *J. Am. Chem. Soc.* **145**, 17845–17855 (2023).
49. Wang, S., Sawada, T., Ohara, K., Yamaguchi, K. & Fujita, M. Capsule–capsule conversion by guest encapsulation. *Angew. Chem. Int. Ed.* **55**, 2063–2066 (2016).
50. Zhang, D. et al. Temperature controls guest uptake and release from Zn_4L_4 tetrahedra. *J. Am. Chem. Soc.* **141**, 14534–14538 (2019).
51. Matis, A. & Matis, C. The dual control – a requirement of the current bank management. *Ann. Econ. Ser.* **5**, 71–75 (2014).
52. Feldbaum, A. A. Dual control theory. I. *Avtomat. i Telemekh.* **21**, 1240–1249 (1960).
53. Filatov, N. M., Keuchel, U. & Unbehauen, H. Dual control for an unstable mechanical plant. *IEEE Contr. Syst. Mag.* **16**, 31–37 (1996).
54. Gilman, A. G. G proteins and dual control of adenylate cyclase. *Cell* **36**, 577–579 (1984).
55. Greenwood, E. Dual control. *Nat. Rev. Genet.* **3**, 731 (2002).
56. Badeau, B. A., Comerford, M. P., Arakawa, C. K., Shadish, J. A. & DeForest, C. A. Engineered modular biomaterial logic gates for environmentally triggered therapeutic delivery. *Nat. Chem.* **10**, 251–258 (2018).
57. Zhang, P. et al. A programmable polymer library that enables the construction of stimuli-responsive nanocarriers containing logic gates. *Nat. Chem.* **12**, 381–390 (2020).
58. Angelos, S., Yang, Y.-W., Khashab, N. M., Stoddart, J. F. & Zink, J. I. Dual-controlled nanoparticles exhibiting AND logic. *J. Am. Chem. Soc.* **131**, 11344–11346 (2009).
59. Shi, P., Ju, E., Ren, J. & Qu, X. Near-infrared light-encoded orthogonally triggered and logical intracellular release using gold nanocage@smart polymer shell. *Adv. Funct. Mater.* **24**, 826–834 (2014).
60. Xu, C. et al. Bioinspired mechano-sensitive macroporous ceramic sponge for logical drug and cell delivery. *Adv. Sci.* **4**, 1600410–1600418 (2017).
61. Kim, Y.-H. & Tabata, Y. Dual-controlled release system of drugs for bone regeneration. *Adv. Drug Deliv. Rev.* **94**, 28–40 (2015).
62. Fu, W. et al. Dual photo-controlled release system for fipronil and dinotefuran. *Photochem. Photobiol. Sci.* **22**, 825–836 (2023).
63. Lakkireddy, H. R. & Bazile, D. V. Nano-carriers for drug routeing – towards a new era. *J. Drug Target.* **27**, 525–541 (2019).
64. Hirao, T. et al. Control over multiple molecular states with directional changes driven by molecular recognition. *Nat. Commun.* **9**, 823–831 (2018).
65. Kobayashi, K. & Yamanaka, M. Self-assembled capsules based on tetrafunctionalized calix[4]resorcinarene cavitands. *Chem. Soc. Rev.* **44**, 449–466 (2015).
66. Fujita, D. et al. Self-assembly of $M_{30}L_{60}$ Icosidodecahedron. *Chem*. **1**, 91–101 (2016).
67. Wu, Y.-T. & Siegel, J. S. Aromatic molecular-bowl hydrocarbons: synthetic derivatives, their structures, and physical properties. *Chem. Rev.* **106**, 4843–4867 (2006).
68. Szumna, A. Inherently chiral concave molecules—from synthesis to applications. *Chem. Soc. Rev.* **39**, 4274–4285 (2010).
69. Stuparu, M. C. Corannulene: a curved polyarene building block for the construction of functional materials. *Acc. Chem. Res.* **54**, 2858–2870 (2021).

70. Huang, F. et al. Corannulene-based coordination cage with helical bias. *J. Org. Chem.* **83**, 733–739 (2018).
71. Shao, C. et al. Guest differentiation and fingerprinting based on the conformational diversity of a dynamic corannulene-based cage. *Org. Chem. Front.* **10**, 1412–1422 (2023).
72. Introduction to Coordination Chemistry, Lawrance, G. A., Ed., John Wiley & Sons: West Sussex, United Kingdom, 2010.
73. Njogu, E. M., Omondi, B. & Nyamori, V. O. Review: Multimetallic silver(I)–pyridinyl complexes: coordination of silver(I) and luminescence. *J. Coord. Chem.* **68**, 3389–3431 (2015).
74. Morsalia, A. & Masoomib, M. Y. Structures and properties of mercury(II) coordination polymers. *Coord. Chem. Rev.* **253**, 1882–1905 (2009).
75. Ronson, T. K., Wang, Y., Baldridge, K., Siegel, J. S. & Nitschke, J. R. An S_{10}-symmetric 5-fold interlocked [2]catenane. *J. Am. Chem. Soc.* **142**, 10267–10272 (2020).
76. Frisch, M. J. et al. Gaussian 09, revision D.01, Gaussian, Inc.: Wallingford, CT, 2009.
77. Yu, C. et al. Flexible, linear chains act as baffles to inhibit the intramolecular rotation of molecular turnstiles. *J. Am. Chem. Soc.* **138**, 15849–15852 (2016).
78. Anderegg, G. Critical survey of stability constants of EDTA complexes, IUPAC chemical data series-no. 14, Pergamon Press, Oxford (1977).

Acknowledgements

We acknowledge the financial support from the National Natural Science Foundation of China (21971021 and 22371018 to Y.W.; 22271019 to H.J.).

Author contributions

Y. Wang and H. Jiang conceived and designed the experimental studies and supervised the work. Y. Yao, C. Shao., S. Wang, Q. Gong, and J. Liu conducted ligand synthesis and performed complexation studies. Y. Wang conducted computational studies. Y. Wang wrote the paper.

Competing interests

The authors declare no competing interests.

Additional information

Supplementary information The online version contains supplementary material available at https://doi.org/10.1038/s42004-024-01128-z.

Correspondence and requests for materials should be addressed to Hua Jiang or Ying Wang.

Peer review information *Communications Chemistry* thanks the anonymous reviewers for their contribution to the peer review of this work. A peer review file is available.